ACS APPLIED MATERIALS & INTERFACES

Research Article

www.acsami.org

Fullerene Hollow Microspheres Prepared by Bubble-Templates as Sensitive and Selective Electrocatalytic Sensor for Biomolecules

Lang Wei,[†,‡] Yilong Lei,[†] Hongbing Fu,*[,†] and Jiannian Yao[†]

[†]Beijing National Laboratory for Molecular Sciences (BNLMS), Institute of Chemistry, Chinese Academy of Sciences, Beijing, 100190, P. R. China.

[‡]The Graduate University of Chinese Academy of Sciences (GUCAS), Beijing 100049, P. R. China

Supporting Information

ABSTRACT: We developed an electrocatalytic sensor based on C_{60} hollow microspheres for highly sensitive and selective detection of dopamine (DA) in the presence of ascorbic acid (AA), and uric acid (UA) in the presence of L-cysteine (RSH). The hollow microspheres of C_{60} with a diameter controllable in the range of 0.5 to 1.5 μm and a thickness of 200 nm are synthesized by a high-temperature reprecipitation method with the assistance of alcohol bubbles. The superhydrophobicity of C_{60} hollow microspheres makes them capable of forming a compact thin film at air/water interface, which can be readily transferred on the surface of gold or glassy carbon electrodes. This porous C_{60} film made from C_{60} hollow microspheres shows a specific surface area as high as 107 m^2 g^{-1}. In order to obtain a conducting film, the C_{60}-modified electrode is pretreated by scanning the potential range from 0.0 to −1.5 V in 1 M KOH followed by potential cycling between 550 to −50 mV in a pH 7.2 phosphate buffer solution. On the basis of XPS and IR measurements, we found that surface oxides, such as −OH and C═O groups, are introduced on the surfaces of the conducting C_{60} film. This, combined with the porosity that enhances the adsorption activity of C_{60}-modified electrodes, enable the electrocatalytic analysis of target biomolecules with detection limit as low as 0.1 nM for DA in the presence of AA, and 1 μM for UA in the presence of RSH.

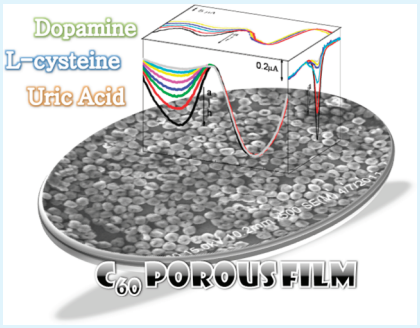

KEYWORDS: *fullerene, hollow microsphere, C_{60}-modified electrode, electrocatalytic analysis, biomolecules*

Fullerene (C_{60})-based materials have been a subject under intensive investigation in the last decades, because of their potential applications in various fields ranging from electronics[1] and photovoltaics[2] to magnetics.[3] Because of the excellent redox property as well as the chemical stability and the biocompatibility,[4] C_{60} has also stimulated considerable research in the electrochemical sensing and analysis of biorelated molecules.[5,6] Typically, C_{60}-modified electrodes were prepared by drop-casting of the C_{60} solution on an underlying support electrode; then the modified surface was pretreated to induce a "partially reduced", conducting C_{60} film, which has been often attributed to the origin of the electrocatalytic activity of C_{60}-modified electrodes. Initially, Szűcs and co-workers proposed that the irreversible reduction of the C_{60} film produces C_{60}^{m-} anions and subsequently results in the formation of electrolyte salts in the modified film,[7] whereas Wildgoose and Compton[8] argued that the reduction actually involves the production of adventitious, polyepoxidated C_{60} ($C_{60}O_n$). However, because of lack of confirmative evidence of the key reactive species, considerable curiousness had been cast on the electrocatalytic orgin of C_{60}-modified electrodes. For example, Banks and co-workers suggested that the electrocatalysis observed for C_{60}-modified electrodes is due to the substrate activation through introduction of surface oxygenated species.[9] Recently, the performance of C_{60}-modified electrochemical sensors has been related to the porosity of the partially reduced C_{60} film.[5] Moreover, Nakashima et al. developed the alternative modified electrode with C_{60} embedded in cationic matrices. Though this special electrode showed a stable electrochemical response, the further applications in devices had not been explored.[10,11] To the best of our knowledge, morphology optimization for the fabrication of high-performance C_{60}-modified electrodes remains largely unexplored.[12] This, together with the uncertainty behind the electrocatalytic mechanism, had severely restricted the application of C_{60}-modified electrodes in analytical electrochemistry.

It should be noted that carbon materials, such as carbon ionic liquid,[13] carbon nanotube,[14] and graphene,[15] are used extensively on electrodes for the electroanalysis of target analytes, which are ultimately utilized to increase selectivity and sensitivity.[16] It is widely accepted that the propensity of carbon to adsorb molecules from solution and the presence of surface oxides at the edge plane of graphite or graphene sheets permit electrocatalytic reactions on these carbon electrodes.[17] However, the common problem of carbon-modified electrodes like ionic liquid, graphene, and graphite is their low sensitivity (detect limit concentrations >1 μM), which may limit their applications in detecting overlapped potential peaks between

Received: December 13, 2011
Accepted: March 5, 2012
Published: March 5, 2012

different analytes, whereas other carbons of, for example, black carbon and nanotube have come from the presence of impurities of, for example, sulfur giving rise to false electrochemical performance.[18] On the other hand, it is well-known that hollow particles, especially those of a spherical geometry, exhibit catalytic activities different from their solid counterparts with the advantages of high surface area and reduction of costs.[19] Herein, we first develop a facile method, namely, the high-temperature reprecipitation technique with the assistance of bubble-template, to synthesize C_{60} hollow microspheres. These C_{60} hollow microspheres with diameter from 0.5 to 1.5 μm and a thickness of 200 nm are capable of forming a compact thin film at air/water interface. The porous C_{60} film shows a specific surface area as high as 107 m^2 g^{-1} and can be readily transferred on the surface of gold or glassy carbon electrode. Second, to obtaining the conducting property, the C_{60}-modified electrode is pretreated by scanning the potential range from 0.0 to −1.5 V in 1 M KOH followed by potential cycling between 550 to −50 mV in a pH 7.2 phosphate buffer solution. On the basis of XPS and IR measurements, we found that surface oxides, such as −OH and C═O groups, are introduced on the surfaces of the conducting C_{60} film. Finally, C_{60}-modified electrodes combined with the porosity that enhances the adsorption activity enable the electrocatalytic analysis of target biomolecules with detection limit as low as 0.1 nM for DA in the presence of AA, and 1 μM for UA in the presence of RSH.

RESULTS AND DISCUSSION

Preparation and Characterization of C_{60} Hollow Microspheres. The key idea of our method for the synthesis of C_{60} hollow microsphere is to bring in ethanol bubbles. In a typical synthesis, 9 mg of C_{60} was added into 5 mL of 1, 2, 4-trimethylbenzene (TMB). The mixture was heated slowly to 120 °C that is above the boiling point of ethanol under proptection of nitrogen and stirred for at least 30 min until a transparent solution was obtained. Then, 10 mL of ethanol (EtOH) as the poor solvent was dropwise injected into the C_{60}/TMB solution as quick as possible. After injection, the heating device was removed. And the whole mixture was cooled to room temperature at a rate of 5 °C/min. The brown-dark precipitates were centrifugally separated from the suspension, and washed with ethanol twice prior to vacuum drying.

Scanning electron microscopy (SEM) image (Figure 1a) depicts the structure and morphology of the resulting C_{60} microparticles. It can be seen that hollow spheres with a diameter of 1 μm (see Figure S1 in the Supporting Information) and a shell thickness of 150−200 nm were obtained. Besides, the shell is incomplete. Almost every hollow sphere has an open pore on the shell surface. Transmission electron microscopy (TEM) image (Figure 1b) shows that the centers of microspheres are brighter than the edges, further confirming that individual C_{60} spheres are hollow structures. Moreover, the shell of C_{60} microspheres seems rather rough consisted of small nanoparticles. In contrast, if EtOH was injected into the C_{60}/TMB solution that was already cooled down to room temperature in advance, solid micorods with a hexagonal cross-section were obtained (Figure 1c). The diameter of hexagonal rods is typically around 5−7 μm, and their length is around 20 μm (see Figure S2 in the Supporting Information). Additionally, magnified SEM image (Figure 1d) reveals that the outer surface is quite smooth through each rod.

Raman, X-ray diffraction (XRD), and Fourier transform infrared (FTIR) spectra were measured for determining the

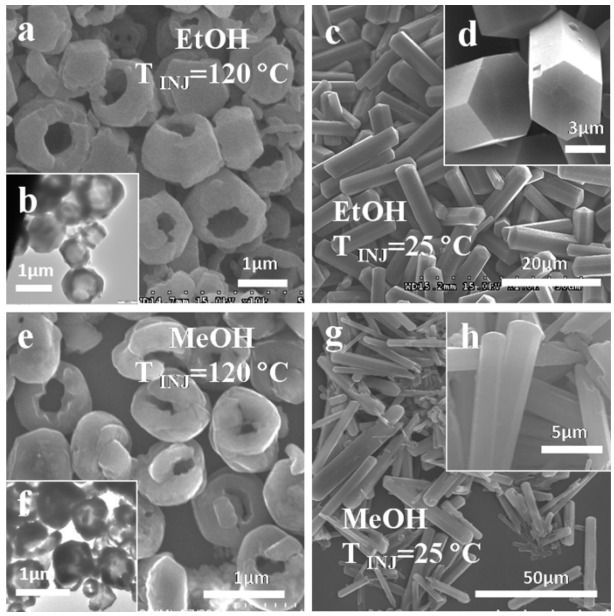

Figure 1. Typical SEM and TEM images of C_{60} microparticles with different shapes from ethanol and methanol at different injection of temperature (T_{INJ}). (a, c, d) SEM and (b) TEM images of C_{60} microparticles with a shape of hollow spheres and rods obtained from ethanol at T_{INJ} = 120 and 25 °C, respectively. (e, g, h) SEM and (f) TEM images of C_{60} microparticles with a shape of hollow spheres and rods obtained from ethanol at T_{INJ} = 120 and 25 °C, respectively.

composition and crystalline nature of hollow spheres and solid rods. Raman spectra of both hollow microspheres and solid rods are in good agreement with that of the pristine C_{60} powder (see Figure S3 in the Supporting Information).[20] The characteristic band for the Ag(2) pentagonal pinch mode, which is known to be sensitive to the intermolecular bonding,[20] is observed at the same position at 1467 cm^{-1} for hollow spheres, solid rods, and the pristine powder. This suggests that molecular C_{60} dominates in these samples and C_{60} polymerization is ignorable. Remarkably, XRD measurements (Figure 2a) verify that hollow structures and solid rods belong to different crystalline phases. The XRD pattern of hollow spheres (middle line) matches well with that of the pristine C_{60} powder (bottom line). Four strong diffraction peaks, corresponding to (111), (220), (222), and (311) crystal planes, can be indexed, according to the fcc lattice parameters.[21] This is in sharp contrast to solid hexagonal rods, which present a XRD curve (top line) entirely different from that of the pristine C_{60} powder (bottom line). Note that incorporation of solvent molecules into the crystal lattices is common for C_{60} crystals grown from solution.[22] Indeed, besides the characteristic absorption of C_{60} at 526, 576, and 1182 cm^{-1},[23] FTIR spectrum of solid hexagonal rods (bottom line in Figure 2b) also presents absorption peaks of TMB at 693, 803, and 876 cm^{-1} (see Figure S4 in the Supporting Information), that actually not detectable in the FTIR spectra of hollow spheres and pristine powder (middle and top lines in Figure 2b). Interestingly, the XRD curve of our hexagonal rods (top line in Figure 2a) is in good agreement with those XRD spectra of rectangular rods and bulk crystals grown from m-xylene solution, which can be indexed to a hexagonal system of rhombohedra structure with cell parameters of $a = b = 23.76$ Å and $c = 10.08$ Å.[24] Although it has not been fully understood yet, we speculate that TMB and *m*-xylene molecules interact with C_{60} in a very similar way

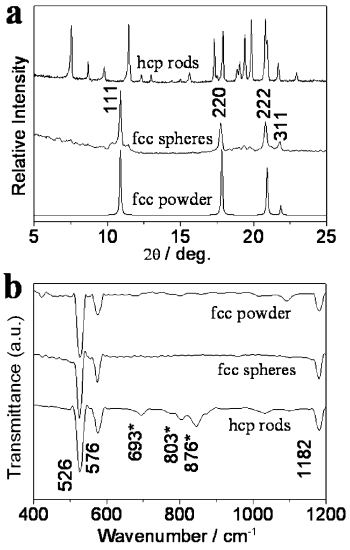

Figure 2. (a) XRD patterns of C_{60} 1D rods, spheres and pristine powder. (b) FTIR absorption spectra of C_{60} rods with hcp phase, spheres with fcc phase, and powder.

in the solid state, driving the C_{60}/TMB crystal falls in the same hcp structure as that of *m*-xylene/C_{60} crystal.

Formation Mechanism of C_{60} Hollow Microspheres. To further probe the formation mechanism of hollow and solid structures, we carefully examined the effect of the injection temperature, T_{INJ}, on both the morphology and crystalline-phase of the resulting particles. A critical point is identified at T_{INJ} = 80 °C, below and above which solid and hollow structures are obtained solely. If 60 °C ≤ T_{INJ} < 80 °C, a mixture of solid particles and short rods showing XRD peaks of both fcc and hcp crystals is observed, whereas uniform solid rods showing only hcp XRD peaks are observed for T_{INJ} ≤ 60 °C. If T_{INJ} ≥ 80 °C, hollow structures that belong to fcc phase are always prepared. Moreover, the shell coverage of hollow structures increases by increasing T_{INJ}. For example, hemirings (Figure 3a), bows (Figure 3b) and hollow microspheres (Figure 3c) were prepared at T_{INJ} = 85, 100, and 160 °C, respectively. On the basis of these results, we proposed a mechanism for the formation of hollow microspheres by virtue of ethanol bubble template (Figure 3d). The driving force for crystallization is generally expressed as $\Delta\mu/k_BT$,[25] where $\Delta\mu$ is

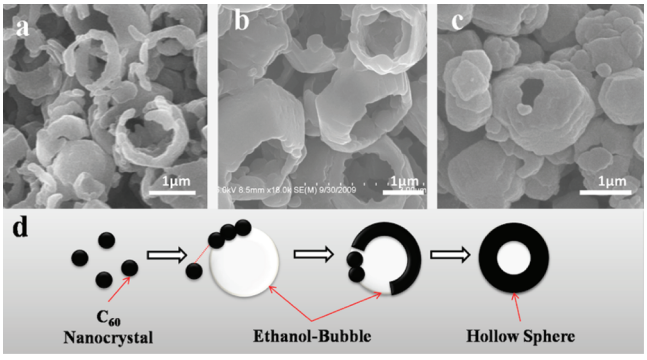

Figure 3. Studies on the plausible mechanism for the formation of C_{60} hollow microspheres. SEM of (a) C_{60} hemi-rings, (b) bows, and (c) almost completely spheres, obtained at T_{INJ} = 85 °C, 100 °C, and 160 °C respectively. T_{INJ}: injection temperature. (d) Plausible mechanism for the formation of C_{60} hollow microspheres with bubble-template.

the difference in chemical potential between the growth units in the crystal and the liquid phase, k_B is the Boltzmann's constant, T is the absolute temperature. And $\Delta\mu$ can be expressed in terms of the supersaturation σ, according to $\Delta\mu = k_BT\ln(\sigma)$ and $\sigma = C/C_{eq}$, where C and C_{eq} represent the actual concentration and the equilibrium concentration of growth units in the coexistence phase. (C_{eq} is also described as the nucleation threshold concentration.) Note that C_{60} are poorly dissolved in common solvents at room temperature. In our method, (i) dissolving of C_{60} was achieved by heating the mixture to the high temperature of 120 °C. This treatment provides high values of C for C_{60}. (ii) Upon quick injection of the poor solvent of EtOH into the TMB solution, the changing of the solvent surroundings as well as the sudden temperature drop from 120 to 90 °C lowers the values of C_{eq} for both tetracene and C_{60}; result in the burst of nucleation.[26] Liu et al. reported that hcp nanorod of *m*-xylene/C_{60} can be transformed to fcc C_{60} nanorod upon heating-treatment above 61 °C as a result of the lose of m-xylene molecules.[24] That is, fcc structure is more thermodynamic stable than hcp structure at high temperature. Therefore, those nanocrystals formed at T_{INJ} ≥ 80 °C in our system are in fcc phase. Meanwhile, the temperature (T_{INJ} ≥ 80 °C) is higher than the ethanol's boiling point (78 °C), thus a boom of ethanol' bubbles are generated. Driven by the minimization of interfacial energy, these fcc nanocrystals have a tendency to aggregate around the bubbles' vapor−solution interface, giving rise to hollow microspheres. This bubble-template mechanism is also evidenced by the fact that below 80 °C only solid structures are formed since ethanol bubbles no longer exist. Note that such kind of aggregation process of nanocrystals with the assistance of bubble templates had also been observed in some inorganic systems.[27] To further testify this bubble-template mechanism, we used methanol to replace the role of ethanol in our preparation. Similarly hollow microspheres (Figure 1e, f) and solid rods (Figure 1g, h) were also obtained at T_{INJ} = 120 and 25 °C, respectively. The diameter of these hollow spheres is around 800 nm, little smaller than those achieved from ethanol. In addition, the results of Raman spectra, XRD patterns and FTIR spectra indicate that the hollow spheres have fcc structure, while the solid rod has hcp structure. Most importantly, the critical point below and above which solid and hollow structures are obtained solely is decreased to 70 °C, which is is a little above the boiling point of methanol (68 °C).

Preparation and Pretreatment of C_{60}-Modified Electrode. Remarkably, these hollow microspheres of C_{60} are found to exhibit superhydrophobicity[28−30] with a water contact angle above 150°. By spreading the dispersion of C_{60} microspheres in ethanol on the water surface, a compact film was formed at the air−water interface (see Figure S5 in the Supporting Information).[31] This film of C_{60} microspheres was uniform and porous with a specific surface area as high as 107 m^2g^{-1} (see Figure S6 in the Supporting Information). Moreover, it can be readily transferred onto any substrate, for example, on the surface of gold (Au) electrode (Figure 4a). The contact angle was measured as 156.3 ± 2 °C. The Au working electrode modified with the film of C_{60} microspheres was then treated according to the procedure reported by Szucs and co-workers,[32] by partially reducing the film in 1.0 mol/L KOH in the potential range of 0.0 to −1.5 V at 10 mV s^{-1} scan rate (see Figure S7 in the Supporting Information). Then, the electrode was equilibrated in phosphate buffer solution of pH 7.2 by cyclic scanning in the potential range of 550 to −50 mV under

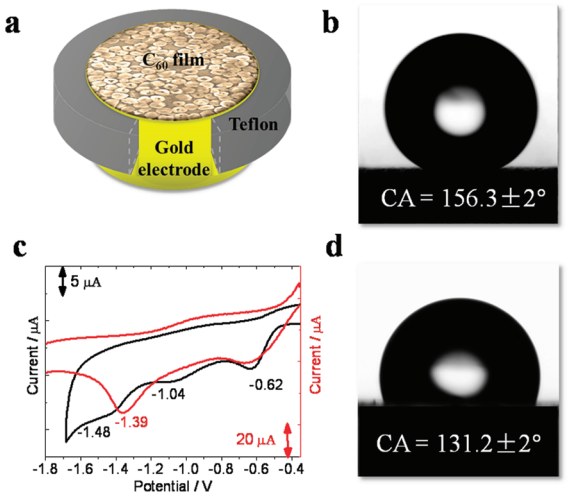

Figure 4. (a) Scheme for the film composed of C_{60} hollow microspheres on gold electrode. (b) The water contact angle of C_{60}-modified electrode before partial reduction. (c) The current voltage of the hydroxylated C_{60} in DMF solution (red line), and after hydroxylated C_{60} removed, the reduction progress of the remained C_{60} in aqueous solutions of 1.0 M KOH with a 10 mV/s rate (black line). Potential vs standard hydrogen electrode (SHE). (d) The water contact angle of C_{60}-modified electrode after partial reduction.

high-purity nitrogen atmosphere. The modified electrode was ready for use.

Surface Structure of C_{60}-Modified Electrode. During the so-called "partial reduction" process of C_{60}-modified electrode, three critical features should be mentioned: (i) as whole process occurred under air conditioning, oxygen and water might be involved that "terminate" the reaction. (ii) In the first scan, a broad peak (ca. 620 mV vs SHE) is indexed to the first reductive peak of C_{60},[4] but no corresponding oxidation wave is observed. (iii) No further voltammetric features are found in subsequent scans (see Figure S7 in the Supporting Information). In the past, these features have simply attributed to the reduction being an electrochemically irreversible process.[7,32] However, after the surface species of C_{60} film was removed by dissolving in N,N-dimethylformamide (DMF) solution, the remained C_{60} modified working electrode again showed three apparent irreversible reduction peaks indexed to C_{60} first, second and third reductive peak (black line in Figure 4c). Interestingly, we investigate the electrochemistry of the surface species using tetra-n-butylammonium hexafluorophosphate as electrolyte; two redox peaks (red line) were obtained. One peak index to 0.62 V consists with the reduction peak of C_{60}, indicating the C_{60} was contained in the surface species. An additional peak index to 1.39 V which could not attributed to C_{60} but agree with the redox of fullerenol ($C_{60}(OH)_8$) in report,[33] suggesting hydroxyl groups (−OH) might included in the surface species. Zhang, et al. proved that C_{60} react with potassium hydroxide (KOH) and oxygen to form polyhydroxylated fullerenes.[34] Further, Previous researcher reported that nearly all carbon surface are prone to reactions with oxygen and water, forming "surface oxides" contained functional groups such as hydroxyl groups (−OH) and carbonyl group (C═O).[17] We further measured the contact angle (CA) of the pretreated C_{60} film, and found the contact angle was decreased to 131.2 ± 2 °C (Figure 4d), which can be attributed to the existence of the hydrophilic groups. The electronic structure of the surface of film was analyzed by measuring the binding energy spectra of C_{1s} and O_{1s} electrons (Figure 5). The X-ray photoelectron spectroscopy (XPS) of the C_{1s} peak is shown in

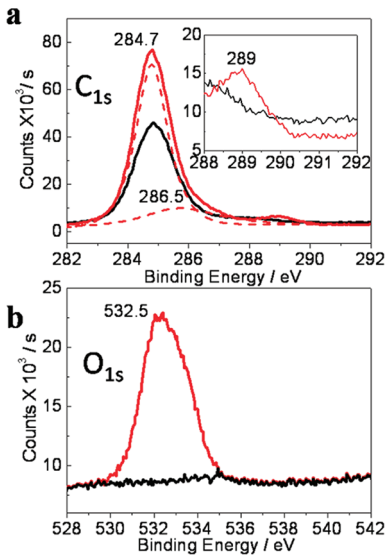

Figure 5. XPS spectrum of (a) C_{1s} and (b) O_{1s} binding energy of C_{60}-film modified electrode.

Figure 5a. The fitted peak with a binding energy at 284.7 eV is assigned to nonoxidized carbon, the peak at 286.5 eV to monooxygenated carbon (C−OH) and the peak at 289.0 eV to deoxygenated carbon (C−O$^-$) (Figure 5a). Another part, the XPS spectrum of O_{1s} (Figure 5b) reveals the peak at 532.5 eV is for O−H. In addition, the IR spectrum of the surface species is shown in Figure S8, a broad O−H band centered at 3440 cm^{-1} is observed, as well as four characteristic bands at 1700, 1635, 1533, and 1429 cm^{-1}, assigned to νC═O, νC═C, δC═C, and δ_sC−O−H absorption. Therefore, we found that surface oxides, including −OH and C═O groups, are introduced on the surfaces of the conducting C_{60} film. Although we have not detected the mechanism yet, we speculate the presence of these surface oxide can have significant electrochemical effects on adsorption and electron transfer rates.[17]

Electroanalytic Activity of C_{60}-Modified Electrode. We modified two kinds of electrodes gold (Au) and glass carbon (GC) to use them detecting four biomolecules: dopamine, ascorbic acid, L-cysteine, and uric acid. Moreover, three desirable characteristics are investigated for examining modified electrodes: (i) Separation of the overlapped voltage potential peaks between different targeting analytes; (ii) increased stability of the electrode response coupled with increments in peak heights facilitating low detection limits; (iii) increased specificity compared to the bare underlying electrode.[35]

Abnormal dopamine (DA) metabolism may lead to certain brain diseases such as schizophrenia and parkinsonism.[36] A major problem of dopamine determination is the disturbance of the coexistence of exccess ascorbic acid (AA), which has the similar oxidized potential to dopamine leading to an overlapping voltammetric response.[36−38] Figure S9a in the Supporting Information shows the differential pulse voltammograms (DPV) of the bare gold (Au) electrode (dashed line) and the hollow-sphere-modified (C_{60}/Au) electrode in the presence of 1.0 mM DA solution in phosphate buffer (pH 7.2). In the case of the bare Au electrode, the electroxidation of DA occurs at ca. 420 mV (vs Ag/AgCl 0.1 *N* HCl). The peak is rather

dx.doi.org/10.1021/am201769u | ACS Appl. Mater. Interfaces 2012, 4, 1594−1600

broad and the current intensity is low at 0.69 μA, suggesting slow electron transfer kinetics. In sharp contrast, a well-defined oxidation peak is obtained at the modified C_{60}/Au electrode. The oxidation peak is negatively shifted to ca.330 mV (vs Ag/AgCl 0.1 *N* HCl) and the peak current increase to 13.5 μA. Similarly, the oxidation peak of ascorbic acid also has a negative shift from ca. 170 to 50 mV (vs Ag/AgCl 0.1 *N* HCl) and receives an enhanced peak current from 0.9 μA to 3.2 μA (see Figure S9b in the Supporting Information). These results point out that the modified C_{60}/Au electrode promoted the electrochemical reaction of both DA and AA. Figure S9c in the Supporting Information shows the square-wave voltammogram (SWV) of 2 μM DA (a know concentration in human body) and 0.5 mM AA coexisted in a 0.1 M phosphate buffer at pH 7.2. The bare Au electrode is unable to separate the responses of DA and AA and detect a single rather broad oxidation peak at ca. 170 mV due to the mixing of indistinguishable oxidation peaks of AA and DA (dashed line). In another case, by using the modified C_{60}/Au electrode, two separate oxidation peaks that can be individually attributed to the oxidation of DA and AA are clearly achieved (solid line).

Figure 6a–d presents the SWVs obtained while changing the concentration of one analyte and keeping the concentration of the other constant. As observed, when the concentration of DA increased, and the peak current of DA increased with the voltammetric peak position unaltered (Figure 6a). The determination of AA limit-detecting concentration is also performed in the similar way. Upon increasing the concentration of AA, the peak current intensity increased without shifting the oxidation voltammetric peak position (Figure 6c). To further quantitatively investigate the detection limit of DA and AA, the voltammetric peak intensities of DA with various concentrations in 0.5 mM AA (Figure 6b) and AA with different concentrations in 0.1 nM DA (Figure 6d) were measured. Three aspects should be noted:. (i) The calibration curves for both DA and AA are kept linear for a certain range of concentrations, and can be expressed by the equation

$$\Delta I_{DA}(\text{nA}) = 0.054 + 0.045C_{DA}\ (R^2 = 0.963)\quad (1 - 10\ \text{nM})$$

$$\Delta I_{DA}(\text{nA}) = 0.079 + 0.0014C_{DA}\ (R^2 = 0.970)\quad (10 - 2000\ \text{nM}) \qquad (1)$$

$$\Delta I_{AA}(\mu\text{A}) = 0.24 + 0.027C_{AA}\ (R^2 = 0.740)\quad (1 - 13\mu\text{M})$$

$$\Delta I_{AA}(\mu\text{A}) = 0.68 + 0.0019C_{AA}\ (R^2 = 0.974)\quad (13 - 500\mu\text{M}) \qquad (2)$$

(ii) The presence of excess of 0.5 mM AA does not bring any noticeable change in the voltammetric response of DA; (iii) As low as 0.1 nM of DA can be feasibly detected, indicating the high sensitivity of our C_{60}/Au-modified electrode, probably due to the high active area provided by microsphere morphology.

Besides sensitive determination of dopamine and ascorbic acid, C_{60} hollow microspheres were also used to modify glass carbon electrode to detect uric acid, the end product of purine nucleotide eatabolism in human system, and L-cysteine,[39] which is widely used in the food industry as an antioxidant.[6] Figure S9d, e in the Supporting Information shows the differential pulse voltammograms (DPV) comparison of the bare glass carbon (GC) electrode (dashed red line) and the hollow-

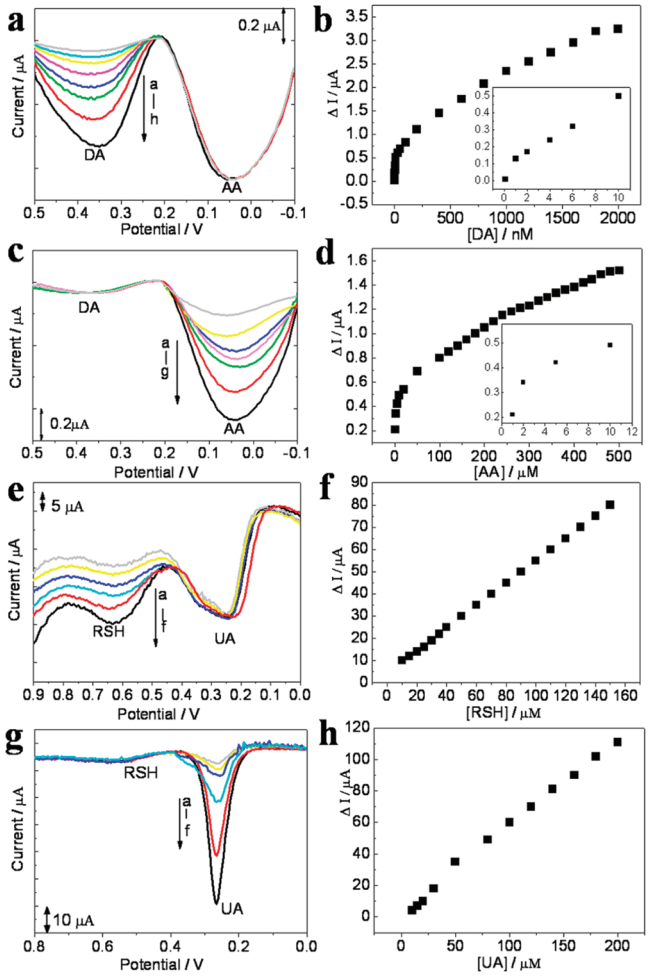

Figure 6. (a–d) Square-wave voltammograms of (a) various concentrations DA at a fixed concentration of AA ([AA] = 0.5 mM [AA]: a = 0.1 nM, b = 0.5 nM, c = 1 nM, d = 2 nM, e = 4 nM, f = 6 nM, g =10 nM, h = 30 nM); (b) relative current intensity vs the concentration of [DA]. Square-wave voltammograms (c) various concentrations AA at a fixed concentration of DA ([DA] = 0.1 nM [AA]: a =1 μM, b = 2 μM, c = 5 μM, d = 10 μM, e = 20 μM, f = 50 μM, g = 100 μM); (d) relative current intensity vs the concentration of AA, DA: dopamine, AA: ascorbic acid; (e–h) Square-wave voltammograms of (e) various concentrations RSH at a fixed concentration of UA ([UA] = 0.08 mM [RSH]: a = 8 μM, b = 10 μM, c = 15 μM, d = 20 μM, e = 25 μM, f = 30 μM); (f) relative current intensity vs the concentration of [RSH]. Square-wave voltammograms: (g) various concentrations of UA at a fixed concentration of RSH ([RSH] = 5 μM [UA]: a = 10 μM, b = 15 μM, c = 20 μM, d = 30 μM, e = 80 μM, f = 100 μM); (h) relative current intensity vs the concentration of UA; RSH, L-cysteine; UA, uric acid.

sphere-modified (C_{60}/GC) electrode (solid black line), detecting 0.05 mM L-cysteine (RSH) solution in phosphate buffer (pH 7.2) and 0.02 mM uric acid (UA) solution in phosphate buffer (pH 7.2), respectively. On the bare GC electrode, the electroxidation of RSH occurs at ca. 850 mV (vs Ag/AgCl 0.1 *N* HCl). The peak is also broad and the current intensity is low of 1 μA. On comparison, a well-defined oxidation peak is obtained at the modified C_{60}/GC electrode. The oxidation peak is negatively shifted to ca.650 mV (vs Ag/AgCl 0.1 *N* HCl) and the peak current increase to 30 μA. Similarly, the oxidation peak of uric acid (UA) also has a negative shift from ca. 500 to 350 mV (vs Ag/AgCl0.1 *N* HCl)

and receives an enhanced peak current from 2 to 10 μA (see Figure S9e in the Supporting Information). These augments identify the modified C_{60}/GC electrode also promoted the electrochemical reaction of both RSH and UA. Further, when detecting low concentration of RSH (0.01 mM) and UA (0.03 mM), the bare GC electrode is unable to reslove the responses of RSH and UA (dash red line in Figure S9f in the Supporting Information). On the contrary, by using the modified C_{60}/GC electrode, two separate oxidation peaks that can be individually attributed to the oxidation of RSH and UA are clearly achieved (solid line). We also present the SWVs obtained while changing the concentration of one analyte and keeping the concentration of the other constant. Note worthily, the calibration curves for both RSH and UA also kept linear for a certain range of concentrations which expressed by the equation

$$\Delta I_{RSH}\ (\mu A) = 4.34 + 0.50C_{RSH}\ (R^2 = 0.999)\ (1 - 200\mu M) \quad (3)$$

$$\Delta I_{UA}(\mu A) = 1.21 + 0.56C_{UA}\ (R^2 = 0.994)\ (1 - 200\mu M) \quad (4)$$

The detailed conditions of all samples in this study are shown in Table 1. Moreover, lowest detection concentration of the each four analytes obtained from the reported C_{60}-film-modified electrode was also concluded in Table 1. The comparison data suggested our proposed electrode system resulted in a better detection limit, higher sensitivity and selectivity of dopamine (0.1 nM) in the presence of ascorbic acid, and L-cysteine (1.0 μM) in the presence of uric acid.

Table 1. Oxidation Voltage, Detection Limit Concentration of Different Samples Using C_{60}-Modified Electrode, and Detection Limit Concentration of C_{60}-Modified Electrodes Reported Earlier

sample	working electrode	oxidation voltage (bare/modified)	detection limit	detection limit earlier reported
dopamine (DA)	gold	0.42/0.33 V	0.1 nM	0.26 nM[5]
ascorbic acid (AA)	gold	0.17/0.05 V	1.0 μM	10.0 μM[5]
L-cysteine (RSH)	GCE	0.85/0.65 V	1.0 μM	20.0 μM[6]
urid Acid (UA)	GCE	0.35/0.25 V	1.0 μM	0.2 μM[39]

Durability and Repetitiveness of C_{60}-Modified Electrode. After the electrochemical experiments, we removed the modified electrode from the solution, and rinsed it in water and ethanol. Then, the detection of the four same biomolecules, dopamine, ascorbic acid, L-cysteine, and uric acid, were performed again. Almost no change in the peak potentials and peak currents was observed, accompanied with the same limit detecting concentration (see Table S1 in the Supporting Information), indicating the repetitiveness of detection obtained from our modified electrode is well. In addition, we exposed the modified electrode to air for a few days, and carried on the same detection in several times. The achieved sensitivity and selectivity suggests the durability of our C_{60} nanosensor is satisfactory.

CONCLUSION

The C_{60} hollow microspheres with a controllable diameter in the range of 0.5−1.5 μm and a thickness of 200 nm are successfully prepared using a high-temperature reprecipitation technique with the assistance of bubble-template. A condensed thin film formed by self-assembling these hollow microspheres at air/water interface shows a specific surface area as 107 m^2g^{-1}, and can be subsequently transferred on the surface of gold or glassy carbon electrode. After the pretreatment irreversible reduction of C_{60}-film-modified electrodes, −OH and C═O groups were introduces onto the surface of C_{60} film. The porosity and hydroxylation of C_{60} film enabled the modified electrodes have affinity for biomolecules and plays as sensitive sensor for the highly selective testing four biomolecules: dopamine (DA), ascorbic acid (AA), uric acid (UA), and L-cysteine (RSH). The enhanced selectivity of different biomolecules with lower limit detecting concentration obtained by our C_{60}-based electrocatalytic sensor may provide the sensing system broad applications in the fullerene nanotechnology.

EXPERIMENTAL SECTION

Materials. Fullerene (C_{60}, 99.5%), dopamine hydrochloride (DA), ascorbic acid (AA), L-cysteine (RSH) and uric acid (UA) were obtained from Aldrich chemical Co. and used without further purification. 1,2,4-Trimethylbenzene was purchased from ACROS Co. Ethanol was provided by Beijing Chemical Agent Ltd. China. Solutions of DA, AA, RSH, and UA were prepared in double distilled water prior to measurements.

Measurements. The morphologies and sizes of the sample were examined using field emission scanning electron microscopy (FESEM, Hitachi S-4800) at acceleration voltages of 10−15 kV. Prior to analysis, the samples were coated with a thin platinum layer using an Edwards Sputter Coater. TEM images were collected by a JEOL JEM-2011 transmission electron microscopy (TEM). One drop of the as-prepared colloidal dispersion was deposited on a carbon-coated copper grid, left to dry under high vacuum, and then observation was performed at room temperature at an accelerating voltage of 200 kV. FTIR spectrum was obtained with KBr pellet on a Bruker Tensor 27. Raman scattering spectrum was recorded on a Bruker RFS 100 Raman spectrometer with a laser of 1064.4 nm at power density of 50 mW mm^{-2}. X-ray diffraction (XRD) patterns were measured by a D/max 2500 X-ray diffractometer with Cu Kα radiation (λ = 1.54050 Å) operated in the 2θ range from 5 to 40°. The water-repellent of hollow microspheres were characterized using an optical contact-angle meter system (Dataphysics OCA20, Germany). The droplets used for the CA measurement were 4 and 7 mg, respectively. The specific surface area of the fullerene hollow microspheres was monitored with an Automated Surface Area & Pore Size Analyzer (QUADRASORB SI, America, Quantachrome Instruments). The resulting products were pretreated under vacuum at 150 °C for 10 h and detected by employing N_2 BET absorption analyses. X-ray photoelectron spectroscopy data (XPS) were obtained with an ESCALab220i-XL electron spectrometer from VG Scientific using 300WAl Kα radiation.

All the electrochemical experiments were carried out using a electrochemistry station (Model 600D, USA, CHInstruments, Inc.). A conventional three-electrode system was employed, with a platinum wire as an auxiliary electrode and Ag/AgCl 0.1 *N* HCl electrode as reference (0.287 V vs SHE, Model CHI111 CHInstruments, Inc.). The working electrode was bare or C_{60}-modified gold electrode and glass carbon electrode having a diameter ca. 2.0 mm, obtained from Universal Analytical & Testing Instruments Ltd. Phosphate buffers of appropriate pH and ionic strength (0.1 M) were prepared according to the method of Christian and Purdy.[40] All measure experiments were carried out at room temperature of 20 ± 5 °C.

Synthesis Method. Fabrication of C_{60}/Au-modified electrode begins with the step that a stock of C_{60} hollow spheres dispersed in

ethanol was spread onto the water surface. A compact and uniform particle film was formed at the air−water interface. The film was then transferred onto the surface of gold electrode by dip-attach method (see Figure S5b in the Supporting Information) and dried under vacuum at 60 °C. The working electrode with a layer of fullerene hollow spheres was then treated according to the procedure described by Szucs and co-workers,[32] by partially reducing the film of C_{60} microspheres on the electrode surface in 1.0 M KOH in the potential range of 0.0 to −1.5 V at a 10 mV/s scanning rate. After being partially reduced, the modified-electrode is placed in phosphate buffer solution of pH 7.2, which was previously deoxygentated with high purity nitrogen. Finally, the electrode was equilibrated in it by cyclic scanning in the potential range of 550 to −50 mV under a nitrogen atmosphere.

■ ASSOCIATED CONTENT

Supporting Information

Related histograms, Raman and FTIR spectrum of C_{60} hollow microspheres; the scheme of the film modified on fullerene hollow microspheres; Nitrogen absorption−desorption isotherms of C_{60} film; IR spectra of C_{60} obtained from C_{60}-modified electrode after partial reduction; electrochemical detecting for biomolecules, and durable and repetitive test of C_{60}-modified electrode. This material is available free of charge via the Internet at http://pubs.acs.org/.

■ AUTHOR INFORMATION

Corresponding Author

*E-mail: hongbing.fu@iccas.ac.cn.

Notes

The authors declare no competing financial interest.

■ ACKNOWLEDGMENTS

This work was supported by the National Natural Science Foundation of China (20873163, 20373077, 20925309), the Chinese Academy of Sciences ("100 Talents" program), and the National Baisc Research Program of China (973) 2011CB808402.

■ REFERENCES

(1) Itaka, K.; Yamashiro, M.; Yamaguchi, J.; Haemori, M.; Yaginuma, S.; Matsumoto, Y.; Kondo, M.; Koinuma, H. *Adv. Mater.* **2006**, *18*, 1713.
(2) Brabec, C. J.; Heeney, M.; McCulloch, I.; Nelson. *J. Chem. Soc. Rev.* **2011**, *40*, 1185.
(3) Stephens, P. W.; Cox, D.; Lauher, J. W.; Mihaly, L.; Wiley, J. B.; Allemand, P.-M.; Hirsch, A.; Holczer, K.; Li, Q.; Thompson, J. D.; Wud, F. *Nature* **1992**, *355*, 331.
(4) Echegoyen, L.; Echegoyen, L. E. *Acc. Chem. Res.* **1998**, *31*, 593.
(5) Goyal, R. N.; Gupta, V. K.; Bachheti, N.; Sharma, R. A. *Electroanalysis* **2008**, *20*, 757.
(6) Tan, W. T.; Bond, A. M.; Ngooi, S. W.; Lim, E. B.; Goh, J. K. *Anal. Chim. Acta* **2003**, *491*, 181.
(7) Szucs, A.; Tolgyesi, M.; Csiszar, M.; Nagy, J. B.; Novak, M. *Electrochim. Acta* **1998**, *44*, 613.
(8) Doneux, T.; Limon-Petersen, J. G.; Compton, R. G. *Phys. Chem. Chem. Phys.* **2010**, *12*, 15029.
(9) Griese, S.; Kampouris, D.; Kadara, R.; Banks, C. *Electrochim. Acta* **2008**, *53*, 5885.
(10) Nakashima, N.; Tokunaga, T.; Nonaka, Y.; Nakanishi, T.; Murakami, H.; Sagara, T. *Angew. Chem., Int. Ed.* **1998**, *37*, 2671.
(11) Nakanishi, T.; Ohwaki, H.; Tanaka, H.; Murakami, H.; Sagara, T.; Nakashima, N. *J. Phy. Chem. B* **2004**, *108*, 7754.
(12) Babu, S. S.; Möhwald, H.; Nakanishi, T. *Chem. Soc. Rev.* **2010**, *39*, 4021.
(13) Safavi, A.; Maleki, N.; Moradlou, O.; Tajabadi, F. *Anal. Biochem.* **2006**, *359*, 224.
(14) Zhu, H. R.; Wu, W.; Zhang, H.; Fan, L. Z.; Yang, S. H. *Electroanalysis* **2009**, *21*, 2660.
(15) Wang, Y.; Li, Y.; Tang, L.; Lu, J.; Li, J. *Electro. Commun* **2009**, *11*, 889.
(16) Walker, P. L.; Radovic, L. R. *Chemistry and Physics of Carbon: A Series of Advances*; Marcel Dekker: New York, 1991.
(17) McCreery, R. L. *Chem. Rev.* **2008**, *108*, 2646.
(18) Banks, C. E.; Crossley, A.; Salter, C.; Wilkins, S. J.; Compton, R. G. *Angew. Chem., Int. Ed.* **2006**, *45*, 2533.
(19) Xia, Y.; Mokaya, R. *J. Mater. Chem.* **2005**, *15*, 3126.
(20) Iwasa, Y.; Arima, T; Fleming, R. M.; Siegrist, T.; Zhou, O.; Haddon, R. C.; Rothberg, L. J.; Lyons, K. B. Jr.; H., L. C.; Hebard, A. F.; Tycko, R.; Dabbagh, G.; Krajewski, J. J.; Thomas, G. A.; Yagi, T. *Science* **1994**, *264*, 1570.
(21) David, W. I. F.; Ibberson, R. M.; Matthewman, J. C.; Prassides, K.; Dennis, T. J. S.; Hare, J. P.; Kroto, H. W.; Taylor, R.; Walton, D. R. M. *Nature* **1991**, *264*, 1570.
(22) Park, C.; Song, H. J.; Choi, H. C. *Chem. Commun.* **2009**, 4803.
(23) Krätschmer, W.; Lamb, L. D.; Fostiropoulos, K.; Huffman, D. R. *Nature* **1990**, *347*, 354.
(24) Wang, L.; Liu, B.; Liu, D.; Yao, M.; Hou, Y.; Yu, S.; Cui, T.; Li, D.; Zou, G.; Iwasiewicz, A.; Sundqvist, B. *Adv. Mater.* **2006**, *18*, 1883.
(25) *Crystals: Growth, Morphology and Perfection* Sunagawa, I., Ed.; Cambridge University Press: Cambridge, U.K., 2005.
(26) Murray, C. B.; Kagan, C. R. *Rev. Mater. Sci* **2000**, *30*, 545.
(27) Peng, Q.; Dong, Y.; Li, Y. *Angew. Chem., Int. Ed.* **2003**, *42*, 3027.
(28) Nakanishi, T.; Michinobu, T.; Yoshida, K.; Shirahata, N.; Ariga, K.; Möhwald, H.; Kurth, D. G. *Adv. Mater.* **2008**, *20*, 443.
(29) Wang, J.; Shen, Y.; Kessel, S.; Fernandes, P.; Yoshida, K.; Yaga, S.; Kurth, Dirk G.; Möhwald, H.; Nakanishi, T. *Angew. Chem., Int. Ed.* **2009**, *48*, 2166.
(30) Nakanishi, T.; Shen, Y.; Wang, J.; Li, H.; Fernandes, P.; Yoshida, K.; Yagai, S.; Takeuchi, M.; Ariga, K.; Kurth, D. G.; Möhwald, H. *J. Mater. Chem.* **2010**, *20*, 1253.
(31) Shen, Y.; Wang, J.; Kuhlmann, U.; Hildebrandt, P.; Ariga, K.; Mohwald, H.; Kurth, D. G.; Nakanishi, T. *Chem.—Eur. J.* **2009**, *15*, 2763.
(32) Szucs, A.; Loix, A.; Nagy, J. B.; Lamberts, L. *Electroanal. Chem.* **1995**, *397*, 191.
(33) Zhang, G.; Liu, Y.; Liang, D.; Gan, L.; Li, Y. *Angew. Chem., Int. Ed.* **2010**, *49*, 5293.
(34) Zhang, P.; Pan, H.; Liu, D.; Guo, Z.-X.; Zhang, F.; Zhu, D. *Synth. Commun.* **2003**, *33*, 2469.
(35) Griese, S.; Kampouris, D. K.; Kadara, R. O.; Banks, C. E. *Electroanalysis* **2008**, *20*, 1507.
(36) Chiara, G. D.; Imperato, A. *Proc. Natl. Acad. Sci. U.S.A.* **1988**, *85*, 5274.
(37) Behpour, M.; Ghoreishi, S. M.; Honarmand, E.; Salavati-Niasari, M. *J. Electroanal. Chem.* **2011**, *653*, 75.
(38) Li, C. Y.; Cai, Y. J.; Yang, C. H.; Wu, C. H.; Wei, Y.; Wen, T. C.; Wang, T. L.; Shieh, Y. T.; Lin, W. C.; Chen, W. *J. Electrochim. Acta* **2011**, *56*, 1955.
(39) Goyal, R. N.; Gupta, V. K.; Sangal, A.; Bachheti, N. *Electroanalysis* **2005**, *17*, 2217.
(40) Christian, G. D.; Purdy, W. C. *J. Electroanal. Chem.* **1962**, *3*, 363.